The Astrophysical Journal, 962:83 (14pp), 2024 February 10 https://doi.org/10.3847/1538-4357/ad1685

Multiple Habitable Phases on Outer Exosolar Worlds

Viktor Sparrman[1], Sara Bladh[1], and M. J. Way[1,2,3]
[1] Theoretical Astrophysics, Department of Physics and Astronomy, Uppsala University, Uppsala, SE-75120, Sweden; vviikkttoorr@hotmail.com
[2] NASA Goddard Institute for Space Studies, 2880 Broadway, New York, NY 10025, USA
[3] GSFC Sellers Exoplanet Environments Collaboration, NASA Goddard Space Flight Center, MD 20770, USA
Received 2023 September 8; revised 2023 December 8; accepted 2023 December 8; published 2024 February 8

Abstract

As stars evolve to higher luminosities during first ascension of the giant branch, previously frozen terrestrial worlds may thaw and host liquid water on their surfaces. Eventually these outer worlds again become uninhabitable due to receiving too much incident light and their water inventory evaporating. Solar-mass stars experience a sudden decrease in luminosity entering the horizontal branch, which could result in a secondary habitable phase for their outer worlds. The outer worlds' time with habitable surface climates is key in evaluating the possibility of extraterrestrial life arising. The times inside the habitable zone (TIHZ) are calculated for outer worlds orbiting between 5 and 45 au around a Sun-like star. By comparing the TIHZ to time estimates for life to arise on Earth, we evaluate whether such outer worlds are promising candidates in the search for extraterrestrial life. We use two different solar evolution models (PARSEC and Dartmouth) and both optimistic and conservative habitable zone (HZ) definitions. Multiple habitable phases are found for each outer world. Outer worlds with orbits as large as Saturn are found to have a secondary habitable phase which exceeds the first in duration. Generally, the time inside the HZ is found to decrease almost monotonically with orbiting distance. Water loss is calculated after the first habitable phase to determine whether a secondary habitable phase is possible. For all orbiting distances the water loss is insufficient to deplete a water inventory equivalent to that of many moons in the outer solar system.

Unified Astronomy Thesaurus concepts: Astrobiology (74); Exoplanet evolution (491); Exoplanets (498); Habitable planets (695); Natural satellites (Extrasolar) (483); Solar evolution (1492); Evolved stars (481); Horizontal branch stars (746); Habitable zone (696); Red giant branch (1368); Solar analogs (1941); Stellar evolution (1599)

1. Introduction

Studies of extraterrestrial habitability aim to help answer the question of whether there is life in the Universe other than what exists here on Earth. As a measure, habitability is fundamentally a judgment and there are therefore many differing definitions. For example, one needs to clarify if one considers habitability for humans, for aqueous life, or for some other type of life which does not require liquid water to function.

Some studies consider habitability of subsurface oceans encased in ice (e.g., Schulze-Makuch & Irwin 2001), nonwater solvents such as a water-ammonia mix (e.g., Fortes 2000), or liquid nitrogen for silicon-based life (e.g., Bains 2004). However, we will focus on the habitability definition of liquid water existing on a surface with an Earth-like atmosphere of N_2–CO_2–H_2O (e.g., Kasting et al. 1993; Kopparapu et al. 2013) or with the addition of methane (e.g., Ramirez & Kaltenegger 2018). Having selected the aqueous habitability definition also limits the habitability candidates to terrestrial bodies, i.e., either (exo)planets or (exo)moons. There are two noteworthy benefits to this consideration of habitability. First, this constrains the habitability modeling problem to climates similar to our own. Second, Ramirez (2018) argues that the identification of Earth-like climates is easier since it is known what atmospheric spectra such a world would produce. This would aid in detecting possibly habitable worlds in future surveys.

The orbiting distance of a terrestrial world is critical in the evaluation of its habitability, as surface liquid water cannot exist on worlds that orbit too close or too far away from their host star. The liquid water habitable zone (HZ) refers to a range of stellar distances wherein an orbiting body is deemed possibly habitable (Huang 1959). The orbital range definition of the HZ can be extended to stellar systems that differ from one another by instead defining the HZ with respect to the incident starlight (instellation) of the orbiting body and the effective temperature of the star (e.g., Kasting et al. 1993; Selsis et al. 2007; Kopparapu et al. 2013). Adding the effective temperature to the definition of the HZ is necessary to account for wavelength-dependent optical properties of the atmosphere in order to compute an effective instellation received at the surface of the orbiting body.

One can show that if orbiting bodies are bound to a disk then the size of the HZ is proportional to the luminosity of the star (e.g., Huang 1959). When a star evolves over time there are changes to its luminosity and effective temperature and the worlds around the star will shift with respect to the two-parameter definition of the HZ and may either exit or enter the HZ (e.g., Danchi & Lopez 2013; Ramirez & Kaltenegger 2016; Tuchow & Wright 2021, 2023).

For stars similar to the Sun, the HZ is expected to reach the outer stellar system first during the post-main-sequence (post-MS) phases of stellar evolution. The post-MS phases of evolution exhibit rapid changes to luminosity and effective temperature compared to the evolution during the main-sequence (MS) phase (e.g., Carroll & Ostlie 2006). This means that outer worlds are expected to stay within the HZ for a shorter period of time than worlds which are in the HZ during

the MS. Time spent within the HZ increases the probability that life has time to arise on the world (e.g., Westall et al. 2022).

Stars evolve via internal fusion processes, which cause changes to their internal structure and composition. The specific processes, and therefore the evolution of a star, is primarily dependent on its initial stellar mass. Each phase of stellar evolution is characterized by the fusion processes and where they occur in the star. Currently, the Sun is on the MS, defined by core hydrogen burning. We briefly review the post-MS evolutionary phases of a solar-mass star to aid the reader in subsequent discussion of habitability. For a more detailed description, see Prialnik (2000) and Carroll & Ostlie (2006).

Toward the end of the MS phase, the helium produced from hydrogen burning starts to fill the inner core, which is now surrounded by a hydrogen-burning shell. This evolutionary phase is referred to as the red giant branch (RGB; e.g., Salaris et al. 2002). Initially, the luminosity of the star decreases as the region of hydrogen burning is shifted outwards. However, since the mean molecular weight of the star has increased the core contracts and the release of gravitational energy from this contraction accelerates the hydrogen fusion occurring in the shell, increasing the luminosity of the star. The brief decrease in luminosity is referred to as the RGB bump (e.g., Nataf et al. 2013). The core contraction continues as helium is produced and the core eventually becomes electron degenerate. Neutrinos are able to escape from the core of the star, carrying away thermal energy and causing the center to become cooler than the outer parts of the core. Once the outer part of the helium core ignites the triple-alpha helium fusion process, the inner part of the core is heated by this ignition so that on the order of seconds the triple-alpha process ignites in the entire core. This phase is referred to as the helium flash and marks the end of the RGB phase for solar-mass stars.[4] The entire helium flash has a lifetime on the order of 10^5 yr (e.g., Dearborn et al. 2006), which is essentially instant compared to the timescales of the other phases of stellar evolution.

After the helium flash has settled, the star enters the next phase of stellar evolution, known as the horizontal branch (HB), which can be identified by a near-constant luminosity lasting ∼100 Myr. During the HB phase both hydrogen shell fusion and helium core fusion occur simultaneously. Eventually the helium in the core is replaced by heavier elements and the helium fusion moves to a shell surrounding the core. Helium shell burning accompanied by an outer hydrogen-burning shell defines the phase known as the asymptotic giant branch (AGB). Helium burning periodically stops as helium is depleted from the shell, before it starts again once it has been resupplied by the helium produced by the hydrogen-burning shell. The increase in luminosity during the AGB is therefore jagged compared to the monotonic growth during the end of the RGB. During the AGB phase the envelope is ejected via stellar winds, causing significant mass loss. After the AGB phase the star eventually ejects its entire envelope, leaving only the core, known as a white dwarf.

As a parent star evolves, certain orbiting worlds may enter the HZ. The climate evolution of these worlds determines whether they are able to maintain habitability while the host star continues to evolve. Additionally, although a world may lie inside the HZ it may still not have liquid water on its surface for a number of climatic reasons (e.g., Tuchow & Wright 2021). Therefore, one must consider how the climate evolves when evaluating the habitability of a world.

The runaway greenhouse effect, defined by the Simpson–Nakajima limit (Simpson 1929; Nakajima et al. 1992), may arise in a climate where the greenhouse effect is sufficiently strong to vaporize all liquid water. While the climate remains in the runaway greenhouse regime, the water vapor is lost to photodissociation and atmospheric escape (e.g., Watson et al. 1981; Kasting et al. 1993; Goldblatt & Watson 2012; Kuramoto et al. 2013; Lammer et al. 2014). Worlds in a long-term runaway greenhouse state (e.g., Dong et al. 2017; Guo 2019) may lack the necessary water inventory to once again become habitable should their parent star dim to a habitable level. The runaway greenhouse effect may be used to define the inner edge of the HZ (IHZ) as the instellation limit where the climate becomes runaway for any atmospheric composition that is considered.

For the outer edge of the HZ (OHZ), the corresponding instellation limit is the maximum greenhouse effect where an atmospheric composition which maximizes the greenhouse effect still results in a climate that is too cold (e.g., Kasting 1991). For so-called "snowball worlds" with a frozen surface, the surface albedo is higher than if the surface were composed of an ocean (e.g., Goode et al. 2001). Yang et al. (2017) found using a 3D global circulation model (GCM) that to melt such a world may require a critical instellation which is too high for the world to remain habitable once the ice melts and the albedo decreases.

Both the runaway greenhouse effect and glaciation are positive-feedback processes that may destabilize the climate. However, we know that there must exist negative-feedback loops acting to stabilize the climate, as it has for Earth through time. Despite the Sun being roughly 30% fainter 4.5 Gyr ago, the Earth did not exhibit long-term glaciation. This problem is often referred to as the "faint young Sun paradox," and is resolved by the atmospheric greenhouse gas content (mostly carbon dioxide) being much higher during the Archean and regulated through some form of volatile cycling (e.g., Walker et al. 1981; Catling & Zahnle 2020; Charnay et al. 2020).

For the habitability of outer stellar systems there exist two potential candidates which both have a surface and could be sufficiently massive to have an atmosphere: terrestrial exoplanets and large outer moons. To consider terrestrial exoplanets in far-out orbits it is necessary to propose a formation or migration scenario since no terrestrial planets are known to exist in the outer solar system. Additionally, exoplanets in large orbits may lie outside the detection limit of present-day exoplanet surveys (e.g., Borucki et al. 2010; Koch et al. 2010; Howell et al. 2014; Zhu & Dong 2021). Rather than detecting outer terrestrial exoplanets, one might instead infer their existence via simulation (e.g., Ida & Lin 2004). Although outer terrestrial exoplanets have yet to be detected, they appear numerous in simulations and we therefore judge their existence as plausible.

Large exomoons, like terrestrial exoplanets, have yet to be found in distant orbits.[5] However, simulations show that Mars- or even Earth-sized moons could form orbiting or be captured by Jupiter-mass exoplanets (e.g., Heller et al. 2014) and remain on stable orbits for longer than the age of the solar system (Barnes & O'Brien 2002). Heller & Zuluaga (2013) argue that

[4] The helium flash does not occur for sufficiently massive stars.

[5] Within our own solar system it should be noted that Jupiter's moon Ganymede is larger than the terrestrial planet Mercury.

since the exoplanets which could host massive exomoons appear more numerous than Earth-like exoplanets, there might exist more habitable exomoons than habitable exoplanets. However, this is limited by the observational biases for exoplanet detection as well as our constraint on the plausibility of massive exomoons. Future observational searches for exomoons are required to attempt to verify such a claim.

2. Methods

We combine the two-parameter HZ definition with post-MS solar evolution tracks to calculate the time spent inside the HZ as a function of orbiting distance for a stellar system with a Sun-like star. Section 2.1 details and compares the conservative and optimistic instellation limits that are used. Section 2.2 introduces the metric used to evaluate time spent inside the habitable zone. Section 2.3 describes which solar evolution tracks are used and compares the models. Section 2.4 outlines the code and provides equations for the calculation of instellation and water loss. Additionally, as the water loss is dependent on the mass and radius of the world, a selection of hypothetical outer worlds is described.

2.1. Habitable Zone Limits

The HZ limits employed in this work are polynomial fits from the 1D radiative-convective cloud-free climate modeling calculations in Kopparapu et al. (2013). They provide a good first-order starting point for our following analyses. The polynomials are of the form

$$S_{\rm limit} = S_{\rm limit,\odot} + aT_* + bT_*^2 + cT_*^3 + dT_*^4, \quad (1)$$

where the instellation limit $S_{\rm limit}$ is a function of the instellation limit for a solar spectrum, $S_{\rm limit,\odot}$, and the difference in stellar effective temperature from the Sun's effective temperature, $T_* = T_{\rm star} - 5780$ K. The polynomial fits are defined for the stellar effective temperature range from 2600 to 7200 K. The HZ limits are separated into two categories: the "conservative HZ" and the "optimistic HZ." The conservative HZ has its inner edge defined by water loss using either the moist greenhouse or runaway greenhouse limit, whereas its outer edge is defined by the maximum greenhouse effect (see Section 1).

The optimistic HZ is not based on modeling efforts, but rather on inferences of past climate conditions on Venus and Mars. The optimistic IHZ is called the "recent Venus" limit and is defined by the observation that Venus has not had liquid water on its surface in the past billion years (Solomon & Head 1991), corresponding to an instellation limit 1.78 times Earth's current insolation, $S_\oplus$ (1361 W m^{-2}; Coddington et al. 2016). The corresponding optimistic OHZ is similarly defined by the observation that Mars had water on its surface 3.8 Gyr ago (e.g., Tanaka 1986; Kopparapu et al. 2013), when the instellation received was 0.32 times Earth's current insolation (Kopparapu et al. 2013).

It may be noted that the early Mars limit is based on geologic evidence of a warmer and wetter period in the planet's early history (e.g., Haberle 2022). In the recent Venus case the 1.78 $S_\oplus$ instellation limit creates a climate which is too hot in the models of Kopparapu et al. (2013). This result is reflected in the fact that the early Mars limit lies close to the model-derived conservative OHZ limits, whereas the recent Venus limit is comparatively far away from the model-derived IHZ limits (see Figure 1). However, other works (e.g., Yang et al. 2014; Way et al. 2016, 2018; Way & Del Genio 2020) have demonstrated that an early habitable Venus at insolations even greater than 1.78 $S_\oplus$ may be possible, especially for slow rotators such as Venus.

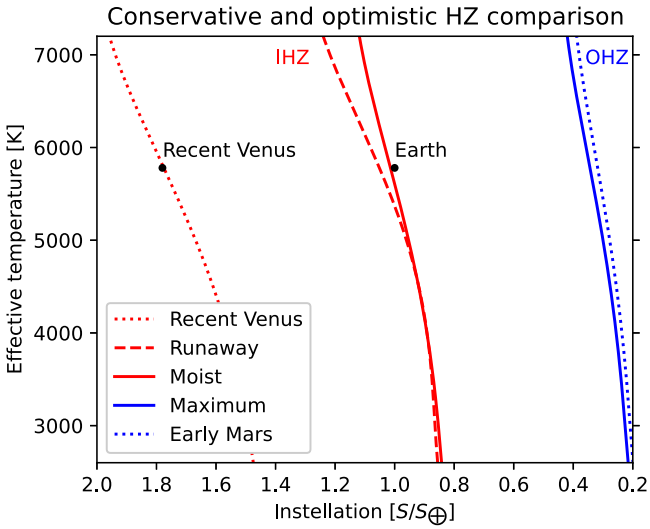

Figure 1. Boundaries of the HZ for various definitions of the HZ using the polynomial (see Equation (1)) fits calculated in Kopparapu et al. (2013). The red lines are the IHZ and the blue lines are the OHZ for different HZ definitions. Data points for current Earth and Venus 1 Gyr ago have been included as a point of reference. The effective temperature covers the entire range of values for which the polynomial fit was defined (2600–7200 K). The x-axis is inverted to preserve the same orientation as if the HZ is defined by orbiting distance rather than instellation. By inverting the axis of the instellation, the IHZ is to the left and the OHZ is to the right.

The rather large IHZ discrepancy between conservative 1D models (e.g., Kopparapu et al. 2013) and 3D GCMs (e.g., Yang et al. 2014; Way et al. 2016, 2018; Way & Del Genio 2020) is due to the inability of 1D models to account for the cooling effects of cloud formation near the substellar point. Way et al. (2018) show that the ability for clouds to cool the climate depends on rotation rate by achieving net radiative balance at instellations up to 1.2 $S_\oplus$ for modern Earth rotation rates and a staggering 2.5 $S_\oplus$ for exoplanets with a sidereal rotation period of 256 Earth days. The equilibrium global mean surface temperature reached in the latter case was ∼310 K. For reference, Venus' current insolation is ∼1.9 $S_\oplus$ and its sidereal rotation period is ∼243 days.

The primary targets of this study, outer exoplanets, may be less likely to be slowly rotating or tidally locked to their host stars (assuming solid-body tidal dissipation is the main cause) due to their larger orbiting distance. However, due to the diversity already observed in exosolar systems (for example, hot Jupiters which do not exist in the solar system), we do not assume that all exosolar systems will be fully alike our own. Just as we do not limit the outer exoplanets to gas and ice giants, we also do not limit them to being fast rotators like the outer planets of the solar system. Slow rotation can also be achieved without tidal locking. The most common explanation for Uranus' high obliquity is by giant impacts at the end of the accretion phase (e.g., Morbidelli et al. 2012; Izidoro et al. 2015; Ida et al. 2020; Salmon & Canup 2022), although other theories have been proposed such as the orbital migration of a satellite that later collided with Uranus (e.g., Saillenfest et al. 2022). It stands to reason that if Uranus' axial tilt can be altered so

drastically by an impact then a similar impact occurring to an outer terrestrial exoplanet might instead slow its rotation rather than tilt its rotation axis, as previously hypothesized for Venus (e.g., Way & Del Genio 2020, their Section 5). At present, observing the rotation rates of terrestrial exoplanets is on the edge of our observational capabilities even for exoplanets orbiting close to their host star (e.g., Li et al. 2022), and is even harder for outer worlds. Future observations of the rotation rates in exosolar systems may further our understanding of what is possible.

Since the HZ definition relies on an Earth-like atmosphere, icy outer moons may seem like poor candidates for habitability given that the thickness of the atmosphere is limited by the mass of the moon. Climate models which scale the atmospheric pressure by the mass of the body obtain a HZ that is thinner for less massive bodies (e.g., Kopparapu et al. 2014). As a counter-example, Saturn's moon Titan is composed of mostly nitrogen and methane (Lorenz et al. 1997) and has a thicker atmosphere than Earth despite having roughly 40 times less bulk mass (Jacobson et al. 2006). However, even if the atmospheric pressure is kept constant for worlds of different mass, the column depth and scale height of the atmospheres would still differ (e.g., Kopparapu et al. 2013). This causes the atmospheric albedo and greenhouse effect of a less massive body to be increased, shifting both the IHZ and the OHZ outward (e.g., Kasting et al. 1993; Kopparapu et al. 2013). The IHZ is affected more than the OHZ, so the effects combine to make the HZ slightly thinner for less massive worlds.

We elect to focus on the optimistic HZ definition due to the aforementioned inability of conservative 1D models to account for the cooling effects of clouds, which would raise the IHZ instellation limit. As the cooling effects of cloud formation can be rotationally dependent and we do not assume any particular rotation rate for our exosolar worlds, the choice of the optimistic HZ merely aims to reflect that we expect more leniency at the IHZ than what is predicted by the conservative HZ model.

2.2. Time Evaluation of the Habitable Zone

To constrain the time in which life might develop, one needs to choose which metric of time to use in relation to habitability. Analogous to the traditional HZ definition of a stellar distance range, the time aspect can be evaluated by introducing a narrower HZ, called the continuously habitable zone, that is defined as either being habitable since the formation of the stellar system or since the start of habitability (e.g., Hart 1979; Kasting et al. 1993; Tuchow & Wright 2023). One may also consider a smaller timescale to evaluate the HZ. For example, one can say "the 1 Gyr continuously HZ" when referring to the range of stellar distances that have been habitable for the past billion years. Tuchow & Wright (2023) discuss the ambiguities and shortcomings in the definition of the continuously HZ. The concept of "belated" habitability is the opposite of continuous habitability, where belatedly habitable worlds are previously uninhabitable worlds that enter the HZ as the host star evolves (Tuchow & Wright 2021, 2023). Including the concept of belated habitability, the HZ can be decomposed into two regions: the continuously HZ and the belatedly HZ. Therefore, the concept of belated habitability carries the same ambiguities as in the definition of the continuously HZ. Although the outer worlds that we are concerned with will belong to this class of belatedly habitable worlds, one would prefer to use a better metric to assess them as habitability candidates with regard to the time evolution of the solar system.

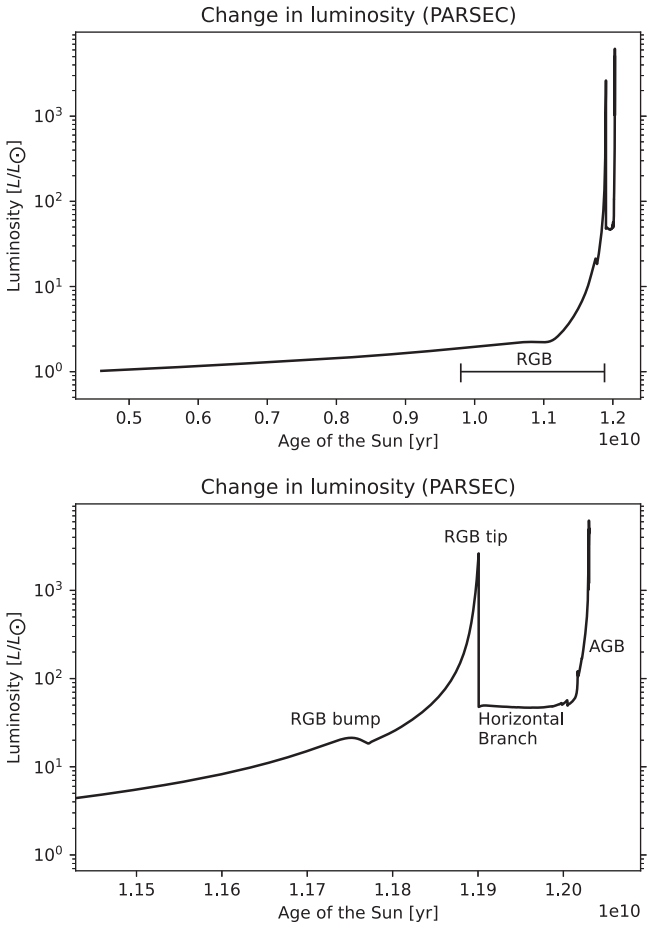

Figure 2. Evolution of luminosity for the Sun until the end of the AGB phase using the PARSEC track. Upper panel: track starts from the current age of the Sun. The RGB is indicated with a span, and the RGB phase begins at $t = 9.8 \times 10^9$ yr. Lower panel: zoom in near the end of the track. The "RGB bump" refers to the visual identification that the luminosity briefly decreases during the RGB phase. The "RGB tip" marks the end of the RGB phase.

There exists another way to evaluate the time aspect of the HZ. Instead of defining a set time in the past from where one imposes habitability and then calculates a stellar range (as is the definition of the continuously HZ), one may instead consider a single fixed stellar distance, e.g., the orbiting radius of some world, and calculate the time span in the habitable zone (TIHZ) as the stellar system evolves (e.g., Danchi & Lopez 2013; Ramirez & Kaltenegger 2016). Danchi & Lopez (2013) calculate the TIHZ for a variety of stellar mass and metallicities, without focusing on post-MS habitability. Ramirez & Kaltenegger (2016), who also employ the TIHZ metric, are specifically concerned with post-MS habitability from the RGB to the AGB. Neither Danchi & Lopez (2013) nor Ramirez & Kaltenegger (2016) examine the occurrence of multiple TIHZs. These are expected since the luminosity of a star is not monotonic in its evolution. For example, for a solar-mass star the RGB phase of stellar evolution has orders-of-magnitude higher luminosity than the subsequent phase, the HB (see Figure 2). Outer worlds with instellations surpassing the IHZ limit at the end of the RGB phase may reenter the HZ during the HB and have a second TIHZ. Calculating multiple TIHZs provides a complete picture of the evolution of

habitability in post-MS stellar systems, which has heretofore been unexplored in prior studies.

We advocate the use of the TIHZ since it can be given as a tuple for bodies which enter and exit the HZ multiple times as their parent star evolves. In this way, the TIHZ captures a more complete description of the stellar system's evolution than the continuously HZ. If one wants to study the possibility of life on a single candidate stellar system at the present day, then the continuously HZ would be sufficient. However, when evaluating the general possibility of extraterrestrial life occurring in a particular type of stellar system, then the presence or absence of numerous TIHZs is relevant for the evaluation. Therefore, the TIHZ metric should be encouraged when evaluating stellar systems as candidates for habitability surveys.

2.3. Track Selection

In order to calculate the TIHZ, one needs the evolution of both parameters of the HZ: the instellation and the effective temperature of the star. Stellar evolution models describe the evolution of a star in terms of its composition and physical characteristics. By matching observed stars to such models, one can determine their age and phase of stellar evolution (e.g., Baraffe et al. 1998, 2015). For our purposes, stellar evolution models provide both effective temperature and luminosity, which can be used to calculate the instellation and in turn the TIHZ as a function of orbiting distance. The stellar evolution models used were the new Padova & Trieste Stellar Evolution Code (PARSEC) v2 tracks[6] (Costa et al. 2019a, 2019b; Nguyen et al. 2022) and the Dartmouth stellar evolution models[7] (Dotter et al. 2007, 2008). PARSEC v2 features numerous improvements over previous versions such as better treating of mixing via stellar rotation and overshooting as well as an updated network of nuclear reactions (e.g., Nguyen et al. 2022). The latter improvement is of particular interest for the purposes of habitability as it results in better reproduction of the observed brightness of the RGB bump phase of stellar evolution (Fu et al. 2018; Costa et al. 2021). In the interest of reproducibility, the stellar tracks used and the code for calculating the TIHZ are available together on Zenodo (Sparrman et al. 2023) and on GitHub.[8]

The solar evolution tracks were pruned to start at the current age of the Sun to cover the future solar evolution through the RGB, HB, and AGB phases of post-MS evolution. While a solar-calibrated track exists for the Dartmouth database, it does not exist yet for v2 of PARSEC. The initial solar metallicity is considered to be $Z_{\odot,\mathrm{ini}} = 0.01774$ by the PARSEC team, whereas the stellar tracks publicly available at the time of writing have a metallicity of at most $Z_{\mathrm{ini}} = 0.017$. A preliminary solar calibration ($Z_{\mathrm{ini}} = 0.01769$) reaching the end of the RGB was generously provided by the PARSEC team to this study for comparison purposes (see the Appendix, Figure 11). The differences between these two tracks are indistinguishable for the purpose of habitability calculations.

Dartmouth and PARSEC also differ in their helium abundance. Both Dartmouth and PARSEC use a linear relation based on a primordial helium abundance of the Sun,

$$Y = Y_{\mathrm{p}} + \frac{\Delta Y}{\Delta Z} Z, \tag{2}$$

but the exact values differ slightly. In the Dartmouth stellar evolution database the primordial helium abundance of $Y_{\mathrm{p}} = 0.245$ uses the first year of Wilkinson Microwave Anisotropy Probe (WMAP) observations (Spergel et al. 2003), while in the PARSEC tracks the primordial helium abundance of $Y_{\mathrm{p}} = 0.2485$ is based on the first 7 yr of WMAP observations (Komatsu et al. 2011). Additionally, the value for the fraction of helium to metal enrichment differs. Dartmouth uses a ratio of $\frac{\Delta Y}{\Delta Z} = 1.6$, while PARSEC uses a ratio of $\frac{\Delta Y}{\Delta Z} = 1.78$. We chose to work with the solar-calibrated track from the Dartmouth database and the closest match to a solar track of $Z_{\mathrm{ini}} = 0.017$ from the PARSEC database without adjustment to align their abundances with each other.

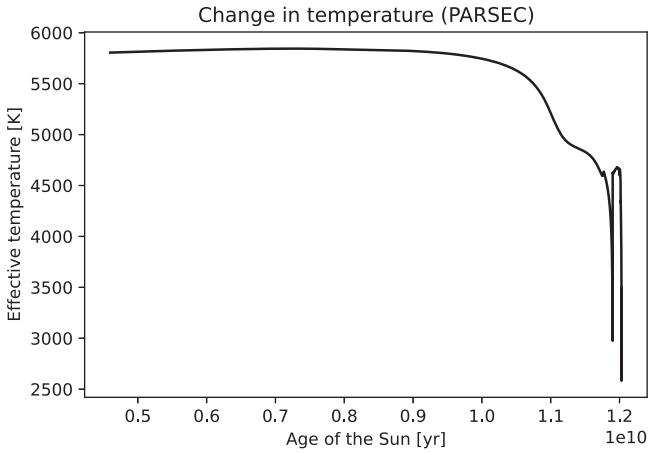

Figure 3. Effective temperature of the Sun (PARSEC track) starting from the current age of the Sun until the end of the AGB phase.

Figures 2 and 3 show the evolution of luminosity and effective temperature in the chosen PARSEC v2 track from the current age of the Sun to the end of the AGB. The evolution of effective temperature and luminosity of the corresponding Dartmouth tracks are similar and can be seen in Figures 12 and 13 in the Appendix. As can be seen on the right side of the upper panel in Figure 2 and the right side of Figure 3, during the late RGB the luminosity and effective temperature of the Sun change rapidly.

Stellar evolution tracks are often separated into MS-RGB and HB-AGB. This is due to the previously described helium flash. Compared to other stages of stellar evolution, the helium flash is several orders of magnitude faster, occurring on timescales on the order of 10^5 yr (Dearborn et al. 2006). This poses a problem in stellar evolution modeling that is resolved in Dartmouth and PARSEC by skipping the helium flash and resuming the stellar evolution after the essentially instant jump to the quiescent helium fusion of the HB phase. Therefore, both the Dartmouth and PARSEC tracks have to be prepared manually by concatenating the HB-AGB tracks to the end of the corresponding MS-RGB track.

2.4. Code Description

All calculations and plots were performed in Python v3 (Van Rossum & Drake 2009). First, the stellar evolution tracks from

[6] http://stev.oapd.inaf.it/PARSEC
[7] http://stellar.dartmouth.edu/models/
[8] https://github.com/Falondil/master

either PARSEC v2 (Costa et al. 2019a, 2019b; Nguyen et al. 2022) or Dartmouth (Dotter et al. 2007, 2008) are loaded and pruned to start after 4.6 Gyr (current age of the Sun). The conservative and optimistic instellation limits are calculated as a function of the stellar effective temperature range between 2600 and 7200 K. Thereafter, the instellation resulting from the evolution of luminosity is calculated for a range of distances between 5 and 44 au using the inverse square law:

$$S(r) = \frac{L}{r^2}, \tag{3}$$

where r is the orbital distance of the orbit considered and L is the luminosity of the star, which evolves in time. The calculated instellations are then compared to the instellation limits to determine when each outer world with that orbiting distance would be inside the HZ. The TIHZ is calculated separately for each of the outer worlds by determining each time the HZ boundaries are crossed.

After the first TIHZ during the RGB, the outer worlds surpass the runaway greenhouse limit of Kopparapu et al. (2013), and we assume the surface water inventory becomes water vapor in the atmosphere. To determine whether the water inventory would disappear before the next possible TIHZ, the time spent with instellation higher than the runaway greenhouse effect is calculated. Since the atmosphere becomes dominated by water vapor in a runaway greenhouse climate, the hydrogen-loss rate will be hydrodynamical (e.g., Watson et al. 1981; Kuramoto et al. 2013; Lammer et al. 2014; Luger et al. 2015; Dong et al. 2017) rather than diffusion limited (e.g., Hunten et al. 1987; Kasting et al. 1993; Guo 2019). The escape rate $\Phi_{\rm esc}$ (number of particles escaping the atmosphere per unit of time),

$$\Phi_{\rm esc} = \frac{4\pi R^3 S_{\rm XUV}}{GMm}, \tag{4}$$

can be calculated using the X-ray and ultraviolet (XUV) instellation $S_{\rm XUV}$, the radius R, the mass of the hydrogen atom m, and the mass of the body M (e.g., Watson et al. 1981; Lammer et al. 2014). In this expression, the radius R is used for both the radius of the body and the radius where most of the XUV flux is absorbed since the height of the atmosphere is assumed to be small in comparison to the radius of the body. Neither PARSEC nor the Dartmouth tracks provide an emitted XUV flux in their model. The emitted XUV flux of a star depends on its rotation speed (which in turn depends on its age) and its mass (e.g., Pizzolato et al. 2003; Ribas et al. 2005; Rybicki 2006; Johnstone et al. 2021). Ribas et al. (2005) compute a power-law fit for the evolution of the XUV flux of a Sun-like star using an observational sample of Sun-like stars. Unfortunately, the oldest star in the sample is younger than the time at which the PARSEC and Dartmouth tracks enter the RGB. Rather than extending the power-law fit beyond its defined interval, we opt for another approach. Rybicki (2006) compute the XUV flux during the RGB tip to be one millionth the total flux. At the start of the RGB the XUV fraction is instead 5.5×10^{-6}. As will be seen in the Results (Section 3), the outer worlds receive a runaway greenhouse climate instellation much closer to the RGB tip than to the start of the RGB phase. Therefore, we use the XUV fraction during the RGB tip to calculate the water loss as the star evolves in both the Dartmouth and PARSEC tracks.

To calculate the total number of escaped particles, one can integrate the escape rate over the time that the world is in a runaway climate:

$$N_{\rm esc} = \int_{t_1}^{t_2} \Phi_{\rm esc}\, dt. \tag{5}$$

Since the precise starting water inventory of the outer worlds is uncertain, we use Earth as a reference. Dividing Equation (5) by the number of hydrogen atoms in Earth's oceans (approximately 10^{47}), one can find the number of Earth oceans lost:

$$\frac{N_{\rm esc}}{N_\oplus} = \frac{\int_{t_1}^{t_2} \Phi_{\rm esc}\, dt}{10^{47}}. \tag{6}$$

This can be used to judge whether we consider a secondary TIHZ to be plausible. Therefore, in order to have the possibility of a secondary TIHZ, one can determine how many Earth oceans the outer world would have to have as an initial water inventory from the time spent in a runaway greenhouse climate.

The mass and radius dependence of Equation (4) is accounted for by computing the escape rate for a set of orbiting worlds having masses and radii which roughly corresponds to the masses and radii of the Moon, Mars, and Earth ($M = [0.01, 0.1, 1.0]\, M_\oplus$ and $R = [0.273, 0.531, 1.0]\, R_\oplus$). The escape rate was also calculated for a hypothetical 5 $M_\oplus$, 1.5 $R_\oplus$ super-Earth. The choice of 5 $M_\oplus$ for the super-Earth is used as an approximate midpoint between the mass of Earth and the mass of 10 $M_\oplus$ after which icy or rocky terrestrials appear less numerous (e.g., Ida & Lin 2004). The 5 $M_\oplus$, 1.5 $R_\oplus$ super-Earth example corresponds to an average density ∼1.5 &times that of Earth.

3. Results

We focus our presentation of results on the PARSEC stellar evolution model as it is newer and the results between models are similar. Whenever the differences between PARSEC and Dartmouth are noteworthy, Dartmouth is also plotted for comparison purposes. Both the conservative and optimistic HZ definitions of Kopparapu et al. (2013) are used in most figures, although for those which only use one HZ definition we have chosen to use the optimistic HZ definition. Several plots feature hypothetical outer worlds with the same stellar distances as the outer planets of the solar system to act as a point of reference, which aims to help the reader understand the results. For example, phrases such as "Jupiter lies inside the HZ" should be interpreted as shorthand for "an outer exosolar world (around a Sun-like star) at the orbiting distance of Jupiter lies inside the HZ."

In Section 3.1 the instellation calculated from the solar evolution models is combined with the instellation limits of the HZ to show at which stellar evolutionary phases outer worlds are expected to be habitable. Section 3.2 details the duration of the TIHZs and also shows the results from the water-loss calculation.

3.1. Passing through the Habitable Zone

The evolution of luminosity (Figure 2) can be used to calculate the evolution of instellation at each outer planet by using the inverse square law (Equation (3)). By using the evolution of the effective temperature (see Figure 3), one can

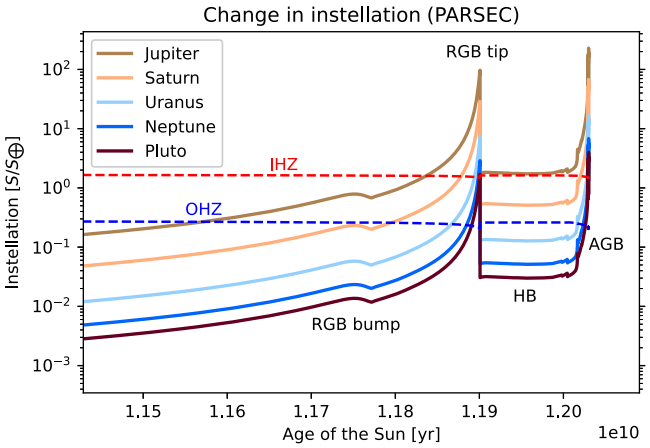

Figure 4. Instellation received at the top of the atmosphere at the orbiting distance of each of the outer planets as the Sun evolves during the RGB to the end of the AGB. Dotted red and blue lines correspond to the instellation limit for the optimistic IHZ and OHZ, respectively. The IHZ and OHZ limits are calculated using the effective temperature for each point in time (see Figures 1 and 3).

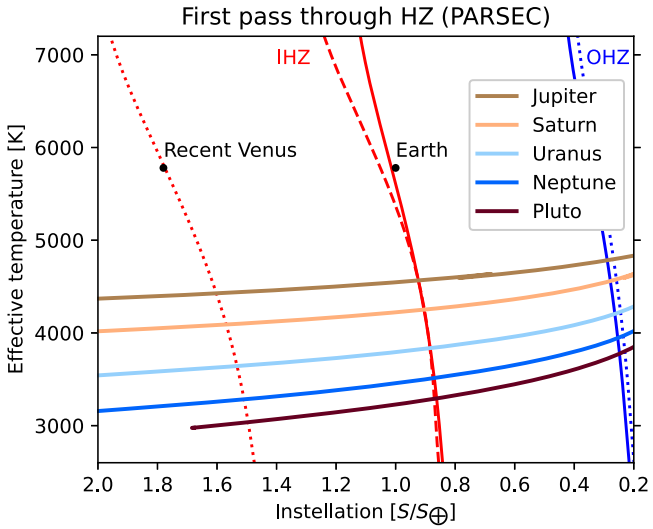

Figure 5. Plot of the various HZ limits (solid red and blue lines) and the evolution of instellation and effective temperature at the orbiting distance of each of the outer planets from the current age of the Sun until the RGB tip (see Figure 2). The HZ limit colors and line styles are the same as in Figure 1. During the RGB the instellation increases and the effective temperature decreases with respect to time. Therefore, the tracks evolve such that they enter from the right side and exit at the left side of the figure. Pluto's track ends inside the axis limits, meaning that Pluto barely exceeds the recent Venus IHZ limit during the RGB.

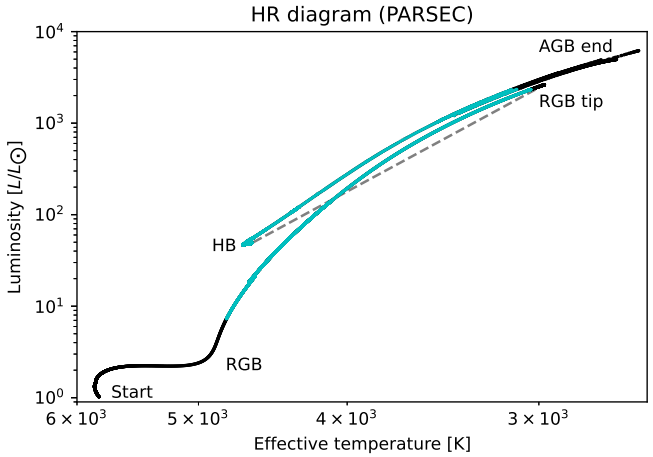

Figure 6. HR diagram corresponding to the PARSEC stellar evolutionary track closest to the Sun ($Z_{ini} = 0.017$) from the current age of the Sun (labeled "Start") to the end of the AGB. Both axes are logarithmic. Cyan markings on the track correspond to times where at least a part of the outer solar system (between 5 and 44 au) lies inside the optimistic HZ. Dotted gray lines trace between the RGB tip and the start of the HB to signify that the RGB helium flash is not resolved in the PARSEC model.

also calculate the instellation limits for the HZ at a given time in the evolution of the star (Equation (1)). Figure 4 compares the instellation received at each of the outer planets to the optimistic HZ instellation limits as a function of time. These HZ limits may appear constant but are in fact functions of the effective temperature of the star at that point in time and therefore evolve slightly. Whenever the outer planet instellations lie between the dotted HZ limits, that planet's orbiting distance is inside the optimistic HZ. The planets first enter the HZ as their instellations reach the OHZ instellation limit (blue dotted line; Figure 4) and then exit the HZ once their instellations exceed the IHZ instellation limit (red dotted line; Figure 4). This is the first TIHZ, and all planets can be seen to have their first TIHZ prior to the RGB tip. Only the optimistic HZ limits are plotted to avoid clutter. If the conservative HZ limits were used instead then the IHZ line would be shifted downward and the OHZ line shifted slightly upward, but this would not affect the presence of a first TIHZ prior to the RGB tip. After the RGB, all planets except Jupiter experience a second TIHZ either during the HB (Saturn) or during the early AGB (Uranus, Neptune, Pluto). It is possible that the planets have more than two TIHZs as the AGB phase is pulsating and periodically exhibits decreases in luminosity. If these occur right after a planet exceeds the IHZ instellation limit then it is possible that the decrease in luminosity temporarily places the planet back inside the HZ. For the interested reader, the same figure using the Dartmouth track instead is available in the Appendix (Figure 14).

The first pass through the HZ, which occurs before the RGB tip, can be seen in Figure 5. In this evolutionary phase, instellation grows with respect to time so the tracks should be interpreted as entering from the right edge of the plot and exiting through the left. All planet tracks appear nearly flat, meaning that during the planets' TIHZs the effective temperature of the star changes much less than the instellation. For all outer planets this first TIHZ occurs at stellar effective temperatures below 5000 K with an inverse relation between effective temperature and orbiting radius. For these temperatures, the width of both the conservative HZ (solid red and blue lines; Figure 5) and the optimistic HZ (dotted red and blue lines; Figure 5) appear to be near constant. What can also be seen is that Pluto only barely receives too much instellation before the end of the RGB, at which point the track is no longer plotted. As such, a body which orbits further out than Pluto—and therefore receives a lower instellation maximum—would not utilize the full width of the HZ since it would not reach the IHZ during the RGB. Worlds in orbits outside $\gtrsim$100 au would never exceed the OHZ limit and therefore never enter the HZ. This would be the case for the proposed giant "Planet X" (e.g., Harrington 1988; Trujillo & Sheppard 2014; Batygin & Brown 2016; Brown & Batygin 2016; Sheppard & Trujillo 2016).

Figure 6 shows the PARSEC track on the Hertzsprung–Russell (HR) diagram from the current age of the Sun until the

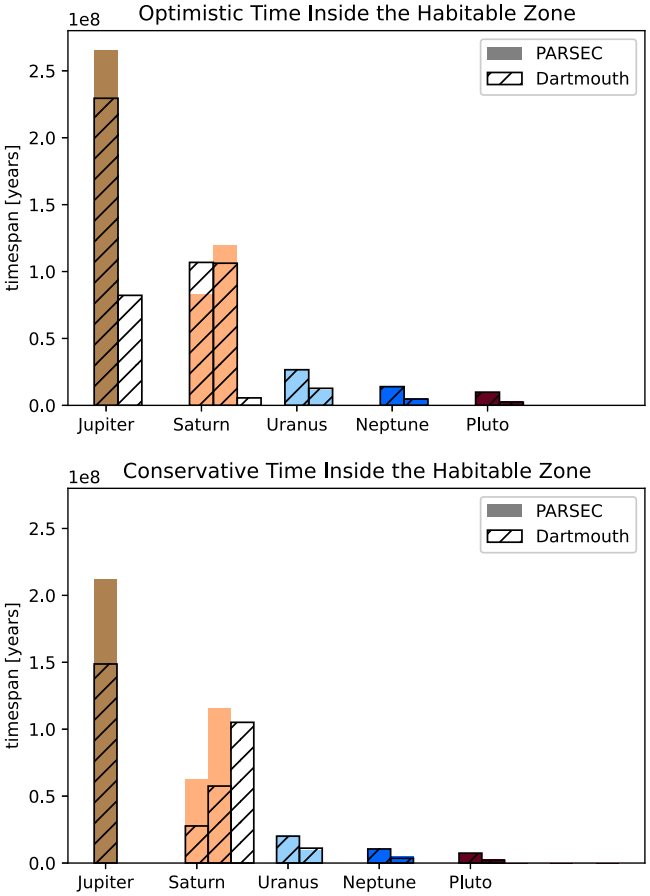

Figure 7. Bar plots of the TIHZs for each of the outer planets using either the PARSEC stellar track with $Z_{ini} = 0.017$ (solid color) or the Dartmouth stellar track (dashed). For planets with several passes through the HZ, the TIHZs appear in chronological order, from left to right, such that the leftmost TIHZ is the one which occurs first (during the RGB; see also Figure 5). Upper panel: optimistic HZ definition. Lower panel: conservative HZ definition.

end of the AGB. The cyan color shows during which stages of stellar evolution (from the middle of the RGB to the late AGB) that at least a part of the outer solar system resides within the optimistic habitable zone. Note that although the track is colored cyan from the start of the RGB to the AGB, no single outer world remains habitable during all of these phases of stellar evolution. Instead, Figure 6 merely implies that the optimistic HZ moves around in the outer stellar system during these phases of stellar evolution.

3.2. Time Span in the Habitable Zone and Water Loss

The outer planets' TIHZs can be seen in Figure 7 as calculated using the optimistic and the conservative HZ definition for both the PARSEC and the Dartmouth tracks. Several TIHZs are shown for each outer planet. In the upper panel of Figure 7, one can notice that Jupiter has an entire secondary TIHZ when using the Dartmouth track which does not exist when using the PARSEC track. This is explained by a difference between the stellar evolution models wherein the HB luminosity is slightly higher for the PARSEC track (see Figure 4) than for the Dartmouth track (see Figure 14 in the Appendix), causing Jupiter to either be inside the HZ for the duration of the HB or not. As seen in the lower panel of Figure 7, Saturn has three TIHZs, which grow in reverse chronological order. In the Dartmouth track, Saturn briefly exits the conservative HZ at the local minimum luminosity of the RGB bump (see Figure 14 in the Appendix) for only 2 Myr before reentering the HZ (see Figure 15 in the Appendix). As can be seen by these examples, when using the outer planets as a proxy for their stellar distance in hopes of generalizing the results to extrasolar systems, one is often susceptible to features which would not exist for an outer world with very slightly different parameters.

Table 1 shows the same TIHZs as Figure 7. As expected, the optimistic TIHZs are slightly longer than the corresponding conservative TIHZs for each outer planet. However, Saturn's TIHZ during the HB (see Figure 4) of ∼110–120 Myr appears independent of the HZ definition used. This reflects the fact that the HB is bounded on either side by sharp increases in luminosity. As such, any planet which lies inside the HZ during the HB will have its TIHZ be insensitive to HZ width and therefore the HZ definition used. Instead, the HB TIHZ matches the duration of the HB, which is ∼100 Myr for all stars that have a HB phase (e.g., Iben 1974; Carroll & Ostlie 2006).

A general trend appears wherein the planets further away from the Sun have shorter TIHZs. However, using merely the orbiting distances where our planets lie to calculate the TIHZs is not sufficient to generalize such trends to other stellar systems. Figure 8 shows the sum of all optimistic TIHZs as a function of orbiting distance for the PARSEC track (upper panel) and the Dartmouth track (lower panel). The vertical lines indicate the orbiting distances of the outer planets in our solar system. Therefore, the upper panel of the previously discussed Figure 7 is a subset of Figure 8. Generally, the sum of all optimistic TIHZs decreases with respect to orbiting distance for both the PARSEC and the Dartmouth tracks. Looking only at the light blue part of Figure 8 (corresponding to the first TIHZ during the RGB) shows how the first TIHZ also decreases for increasing orbital radius. The decrease appears almost monotonic except for an orbiting distance near Saturn, where the second TIHZ (dark blue) suddenly becomes longer than the first TIHZ (light blue). This sharp decrease in the first TIHZ is in fact the RGB TIHZ being split into two nearly consecutive TIHZs (one light blue and one dark blue) at the specific orbiting distances where the peak of the RGB bump is inside the HZ. In the PARSEC track, this RGB bump occurs at lower luminosities than in the Dartmouth track (compare Figure 4 with Figure 14 in the Appendix). For Saturn, the RGB bump occurs prior to the first TIHZ in the PARSEC track and during the first TIHZ in the Dartmouth track. Therefore, in the PARSEC track (Figure 8, upper panel) the discontinuity in the first TIHZ occurs at orbiting radii slightly smaller than that of Saturn, and vice versa for the Dartmouth track.

Water loss on an outer world results from time spent with instellation higher than the runaway greenhouse instellation limit (see Section 2.4). The amount of water lost the first time that the runaway greenhouse climate is reached can be seen in Figure 9. The water loss decreases with increasing mass and, as with the TIHZ, the water loss also decreases with increasing orbital distance. At the orbiting distance of Saturn, none of the hypothetical outer worlds lose as much water as there is in Earth's oceans using either the PARSEC or Dartmouth solar evolution models. At most, the outer worlds lose water equivalent to ∼5 Earth oceans in the case of an outer world with the mass of Earth's moon at a stellar distance of Jupiter. Note that since Jupiter does not have a secondary TIHZ in the PARSEC model (see Table 1), this water loss is calculated until

Table 1
TIHZs for the Outer Planets

Planet	PARSEC				Dartmouth			
	Optimistic HZ		Conservative HZ		Optimistic HZ		Conservative HZ	
	RGB (yr)	Post-RGB (yr)	RGB (yr)	Post-RGB (yr)	RGB (yr)	Post-RGB (yr)	RGB[a] (yr)	Post-RGB (yr)
Jupiter	2.7×10^8	…	2.1×10^8	…	2.3×10^8	8.2×10^7	1.5×10^8	…
Saturn	8.3×10^7	1.2×10^8	6.2×10^7	1.2×10^8	1.1×10^8	1.1×10^8	2.8×10^7, 5.8×10^7	1.1×10^8
Uranus	2.7×10^7	1.1×10^7	2.1×10^7	9.1×10^6	2.7×10^7	1.3×10^7	2.0×10^7	1.1×10^7
Neptune	1.4×10^7	5.5×10^6	1.0×10^7	4.6×10^6	1.4×10^7	4.7×10^6	1.1×10^7	3.6×10^6
Pluto	9.8×10^6	3.1×10^6	7.3×10^6	2.5×10^6	9.9×10^6	2.4×10^6	7.4×10^6	2.0×10^6

Notes. Solar evolution tracks are from PARSEC and Dartmouth. Either optimistic or conservative HZ limits are used to calculate the TIHZs. The two largest TIHZs are shown, one occurring before the RGB tip and one occurring after.
[a] Saturn has two conservative TIHZs listed for the RGB of the Dartmouth track. These are barely disjoint, separated by only 2 Myr (see Figure 15 in the Appendix), and are therefore listed side by side.

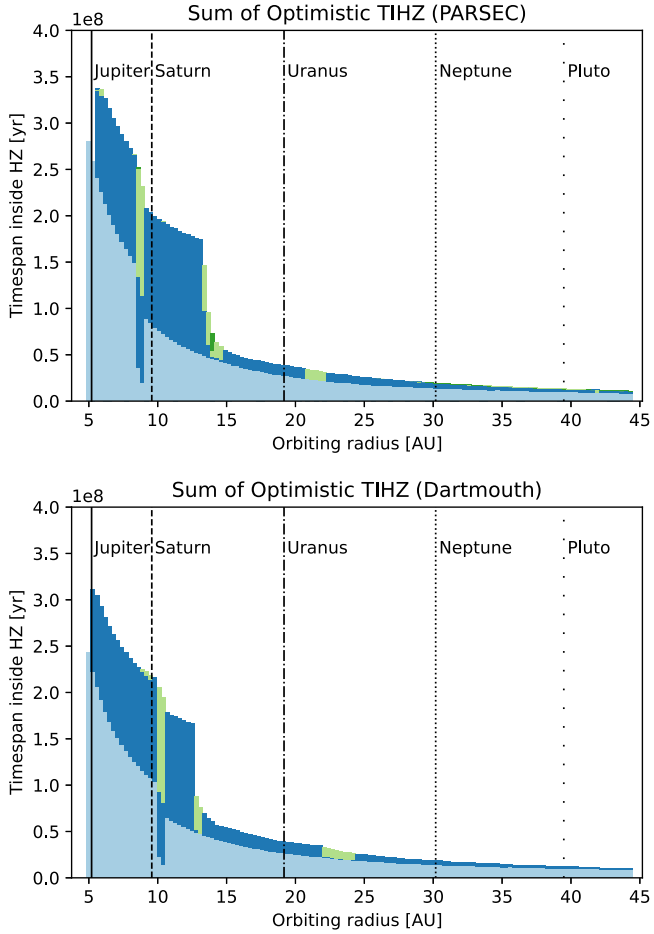

Figure 8. Bar plots of the sum of every optimistic TIHZ for outer worlds around a solar-mass star as a function of their orbiting distance. Vertical lines mark the corresponding orbiting distances of the outer planets to aid the reader. The colors indicate that the TIHZs are disjoint. The first TIHZ is light blue, the second is dark blue, and the third is green. Each TIHZ is added to the plot by stacking it on top of the previous TIHZ. As such, the TIHZs for a particular orbital distance appear chronologically from bottom to top. Upper panel: PARSEC ($Z_{\rm ini} = 0.017$) track. Lower panel: Dartmouth solar track.

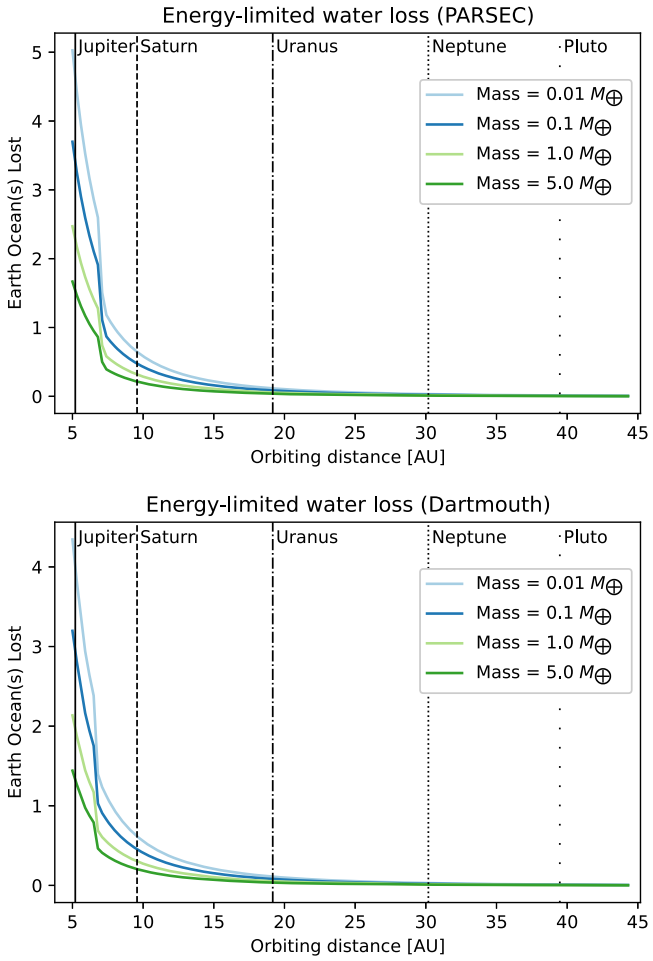

Figure 9. Energy-limited water loss for the outer worlds (see Equations (4) and (6)) using the PARSEC (upper) or Dartmouth (lower) solar evolution model. The water loss is plotted for the time that the instellation exceeds the runaway greenhouse limit prior to the RGB tip. For outer worlds which stay in a runaway greenhouse climate past the RGB tip the water loss is instead calculated until the end of the AGB. The water loss depends on the orbiting distance (x-axis; the orbiting distances of the solar system outer planets are used for reference) and the assumed mass of the hypothetical exosolar world (shown in the legend in units of Earth masses).

the end of the AGB, i.e., for the remainder of the solar evolution track. Yet this water loss is still less than the water inventory of certain outer moons in the solar system such as Ganymede (Grasset et al. 2017).

The greenhouse effect of methane has a positive effect on the radiative balance for worlds where the incident light is from a star with effective temperature $T_{\rm e} \geqslant 4500$ K

(Ramirez & Kaltenegger 2018). Both Jupiter and Saturn enter the HZ from the OHZ side at stellar effective temperatures above 4500 K (see Figure 5). Therefore, the OHZ would be widened, and their TIHZs therefore lengthened, by including the assumption that their moons' atmospheres have a methane component. However, the effect is marginal for stellar effective temperatures close to the threshold of 4500 K below which the effect is reversed.

4. Discussion

The TIHZ for outer worlds is dependent on the stellar evolution track used and the HZ definition that one considers. Despite discrepancies in the models, the PARSEC and the Dartmouth solar tracks appear to have similar evolution in regards to luminosity and therefore instellation. However, the slight differences—as, for example, at what luminosity the RGB bump occurs—can sometimes result in significant differences in the TIHZ and water loss calculated. Similarly, the choice of HZ definition can cause the same effect wherein a significant HB TIHZ is dependent on whether the HZ definition is optimistic or conservative. This effect is caused by the near-constant luminosity of the HB being either included or excluded from the HZ.

Both the TIHZ and the sum of all TIHZs diminish with respect to orbiting distance, which could disfavor outer worlds as habitability candidates. However, the number, surface area, and water inventory of outer exosolar worlds may all exceed that of inner terrestrial exoplanets (e.g., Stern 2003; Heller et al. 2014; Grasset et al. 2017). If life originated in shallow water on the surface of Earth then a larger surface area may increase the probability that life arises, depending upon surface water inventory. Life originating in shallow waters is supported by UV radiation being an energy source able to supply sufficiently high activation energy for starting the prebiotic reaction processes (e.g., Pascal et al. 2013; Pross & Pascal 2013). Even in the solar system, where no terrestrial outer planets have been confirmed (e.g., Harrington 1988; Trujillo & Sheppard 2014; Batygin & Brown 2016; Brown & Batygin 2016; Sheppard & Trujillo 2016), the surface area of the outer moons exceeds that of the inner terrestrial planets (e.g., Stern 2003). Using the solar system as an example again, the water and ice layers of Jupiter's moon Ganymede are 500 km deep, which alone dwarfs the estimated water inventory of Earth by more than an order of magnitude despite Ganymede being much smaller (e.g., Grasset et al. 2017). If the outer regions of exosolar systems are similar to our solar system in both water content and surface area, then outer worlds may be a good place to look for the formation of life. Whether these effects sufficiently counteract the shorter TIHZ is difficult to evaluate rigorously. This is partly due to the outer regions of extrasolar systems being largely unobserved as a result of observational biases which favor bodies close to their host star. Therefore, we do not know how similar the outer regions of extrasolar systems are to our own outer solar system.

4.1. The Emergence of Life

The time for life to arise on Earth can be divided into two parts, the time for Earth to become habitable—which in our definition of habitability simply means surface liquid water—and the time for the habitable Earth to become inhabited. In order to evaluate the TIHZ of outer worlds as significant or insignificant, they should be compared to estimates for the time it takes for life to arise in a habitable climate. Currently, the oldest fossil records are stromatolites, dating back 3.5–3.8 Gyr ago (Schopf et al. 2007). Using this conservative definition, the time for life to arise on Earth is then $\lesssim$1 Gyr since Earth's age is 4.5 Gyr. The main obstacle in either detecting older fossils or deducing water presence is that the rock record from the Hadean (>4.0 Gyr ago) has been lost to tectonic recycling (e.g., Knoll & Nowak 2017; Westall et al. 2022). Zircon crystals have been detected, some as old as 4.4 Gyr (Wilde et al. 2001), that hint at the presence of water (e.g., Knoll & Nowak 2017; Westall et al. 2022). Efforts in modeling the early history of the solar system show that Earth's water inventory was delivered by water from chondritic meteorites, but the exact timing remains uncertain (Kleine et al. 2020). It should be emphasized that the time for life to arise on Earth is only constrained by an upper bound and that the true value for time to arise on the habitable Earth could be many order of magnitudes less than 1 Gyr. Similar in order of magnitude to the aforementioned upper bound, the time for multicellular life to develop on Earth after the Great Oxygenation Event (2.4 Gyr ago) was ~0.8 Gyr (e.g., Knoll & Nowak 2017).

Comparing the TIHZs of the outer worlds (see Figure 8) to the estimated time for life to arise on Earth, one can see that any outer world is in the HZ for less time than the upper bound for the time for life to arise on Earth (although any outer world orbiting closer than Saturn has a TIHZ within an order of magnitude of this upper bound). Pessimistically, if one assumes this upper bound as the limit, it is unlikely that life forms on any one of these outer worlds. However, at least in the case of the solar system, there are many outer worlds. Again, consider life forming as a random event with probability proportional to the habitable surface area. If one defines a random variable X_i to be the the number of times that life forms on the ith outer world in a set time interval, then X_i is Poisson distributed. We will also introduce a random variable Y to be the number of times that life forms on *any* of the outer worlds. The probability that life forms on at least one of the outer worlds is the inverse probability to the event that no life forms on all of them. Therefore, we are interested in evaluating the following probability:

$$\mathrm{P}(Y=0)=\prod_{i=1}^{n} P(X_i=0), \tag{7}$$

where it has been assumed that X_i is independent for all n outer worlds. The above described Poisson distribution can be used to calculate the probability:

$$\mathrm{P}(X_i=0)=\exp\left(-\frac{t_{\mathrm{HZ},i}}{t_{\mathrm{life}}}\frac{A_i}{A_\oplus}\right), \tag{8}$$

where t_{life} is the average time for life to arise on Earth, $t_{\mathrm{HZ},i}$ is the TIHZ of the ith outer world, and A_i and $A_\oplus$ are the areas of the ith outer world and the Earth, respectively. The probability that life forms during any of the outer worlds' TIHZs can then be written as

$$1-\mathrm{P}(Y=0)=1-\exp\left(\frac{-\sum_{i=1}^{n} t_{\mathrm{HZ},i}\,A_i}{t_{\mathrm{life}}\,A_\oplus}\right). \tag{9}$$

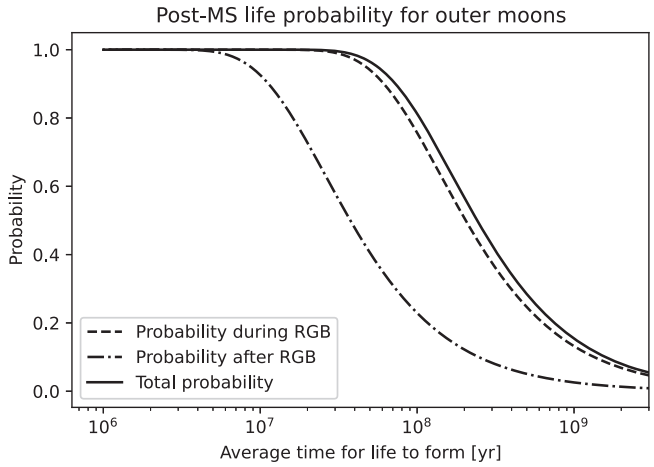

Figure 10. Probability that life forms on any of the outer moons in the solar system as a function of the assumed average time for life to form. The PARSEC solar track and optimistic HZ boundaries are used. All outer moons are assumed to have habitable climates the entire time that they are inside the HZ. Probabilities are separated into the probability that life forms during the RGB (dashed), after the RGB (dashed–dotted), or during either of these phases of stellar evolution (solid).

One could use the upper limit for life's occurrence on Earth to estimate the average time for life to form. However, this value is severely ill-constrained since it is unknown whether the limiting factor for life to develop on Earth was the time before Earth's climate became habitable or the time for the random event that started life. Additionally, it is unknown whether Earth is representative of the time for life to arise since our own existence provides a form of selection bias. Instead, one may consider $t_{\rm life}$ to be an unknown parameter. Since the surface area of outer worlds in some hypothetical extrasolar system is also unknown, we here employ the largest moons and trans-Neptunian objects (TNOs) of the solar system—Jupiter's four largest moons, Saturn's seven largest moons, Triton (the largest moon of Neptune), the five largest moons of Uranus, and the six largest TNOs—to serve as an example. This aims to illustrate the dependence on the quality of outer worlds as habitability candidates on the ill-constrained value of $t_{\rm life}$. It is important to note the crude but necessary assumption that the outer worlds all have a habitable climate for their entire duration inside the HZ. Figure 10 shows how the probability varies using different assumptions for the average time for life to form. We again emphasize that these results are specific to the assumed area and orbit distribution of outer worlds in a stellar system. In this specific case, where we have used the outer moons of the solar system, the resulting probability for time for life to form is seen to be dominated by the RGB TIHZ rather than the HB TIHZ. This is due to Jupiter lacking a HB TIHZ when using the PARSEC model (see Figure 7 and Table 1) and the combined area of Jupiter's moons being larger than the remaining outer worlds in this example case. The code for this calculation is also available on Zenodo so that the reader may freely alter the presumed area distribution of outer worlds.[9]

[9] https://doi.org/10.5281/zenodo.8272045

The HZ is a construct which should be interpreted as a zone where the probability for life to exist is heightened. The atmospheric composition required to maintain habitability at the edges of the HZ is quite distinct from the 1 bar N_2-dominated atmosphere that Earth has had for most of its history. A world near the center of the HZ is more Earth-like and more likely to give rise to life. Whether worlds at the edges of the HZ would be more or less likely to host life is difficult to quantify. However, the TIHZ metric does not distinguish between such worlds. For example, a world which resides at the center of the HZ is evaluated the same as a world which resides at the edge of the HZ for an equal amount of time, although rationally we know that one of these worlds should be judged favorably. The existence of a significant secondary TIHZ for Jupiter using the Dartmouth solar model and optimistic HZ boundaries and the nonexistence of the same TIHZ using the PARSEC solar model (see the upper panel of Figure 7) is a feature of this Boolean property of the HZ. In future studies which focus on comparing the quality of different habitability candidates, one may want to use a weighting factor multiplying the TIHZ that favors worlds near the center of the HZ.

Future work regarding the post-MS habitability of outer worlds could be guided by new 3D climate GCMs, and hopefully the detection of terrestrial worlds in the outer regions of extrasolar systems. Any evaluation of extraterrestrial habitability timescales are currently bounded by our lack of knowledge regarding the timeline for the early climate and formation of life on Earth. Habitability studies would therefore be strengthened by discoveries of older fossils or more conclusive proxies for the climate during the Hadean and the Eoarchean. Additionally, the TIHZ of outer worlds could be explored further by considering host stars with different stellar masses. Since sufficiently massive stars lack a HB, it would be interesting to see whether such stellar systems have any significant secondary TIHZ or are completely dominated by the RGB TIHZ.

5. Conclusion

During the post-MS phases of stellar evolution, outer worlds orbiting a solar-mass star may enter and exit the HZ multiple times. The TIHZ is key in evaluating whether that outer world is a promising candidate for life to form. In general, the TIHZ decreases almost monotonically with orbiting radius. Outer worlds which orbit at a distance such that the near-constant HB luminosity results in habitable instellation have a second TIHZ which exceeds the first. Any subsequent TIHZs are limited by water loss during prior phases of stellar evolution and some form of volatile cycling. The upper limit for water loss between the RGB bump and the AGB is ∼5 Earth oceans, less than the total ice and water inventory of many of the solar system's outer moons. Therefore, energy-limited water loss cannot be used to exclude a secondary TIHZ for outer worlds in exosolar systems similar to our own solar system. All TIHZs calculated are shorter than the time between Earth's formation and the oldest undisputed fossils discovered. However, outer world habitability remains plausible as the time for life to form on Earth is poorly constrained and since the total area of terrestrial outer worlds may be larger than terrestrial worlds in the inner parts of exosolar systems (e.g., Ida & Lin 2004; Heller & Zuluaga 2013). Considering the multitude of outer worlds, the possibility that life forms on any one of them during any of

their TIHZs is sufficient to warrant consideration in the search for extraterrestrial life.

Acknowledgments

This work is partially funded by the Swedish Research Council through grant agreement No. 2021-04510. The authors would like to thank Greg Feiden for discussion regarding stellar evolution tracks, particularly for help with the concatenation procedure after the helium flash. Paola Marigo of Padova University (UNIPD), Chi Thanh Nguyen of Scuola Internazionale Superiore di Studi Avanzati (SISSA), and the PARSEC team are graciously acknowledged for providing the first stellar evolution tracks used in this project prior to the PARSEC v2 release and later providing an as-of-yet unpublished stellar evolution track closer to the Sun's metallicity than what is publicly available. The authors would also like to thank Sonny Harman for guidance regarding water loss. All tracks and code used can be downloaded at https://doi.org/10.5281/zenodo.8272045.

M.J.W. acknowledges support from the GSFC Sellers Exoplanet Environments Collaboration (SEEC) and "ROCKE-3D: The evolution of solar system worlds through time," funded by the NASA Planetary and Earth Science Divisions Internal Scientist Funding Model. This work was also supported by NASA's Nexus for Exoplanet System Science (NExSS) and the NASA Interdisciplinary Consortia for Astrobiology Research (ICAR).

Appendix

A preliminary PARSEC solar calibration track which more closely matches the initial solar metallicity (Z = 0.01774) can be seen in Figure 11 compared to the PARSEC track that was used in this work. Figures 12–14 show the evolution of effective temperature, luminosity, and instellation for the Dartmouth track (equivalent to Figures 2–4 for the PARSEC track). The time between Saturn's TIHZs using the Dartmouth track and the conservative HZ definition can be seen in Figure 15.

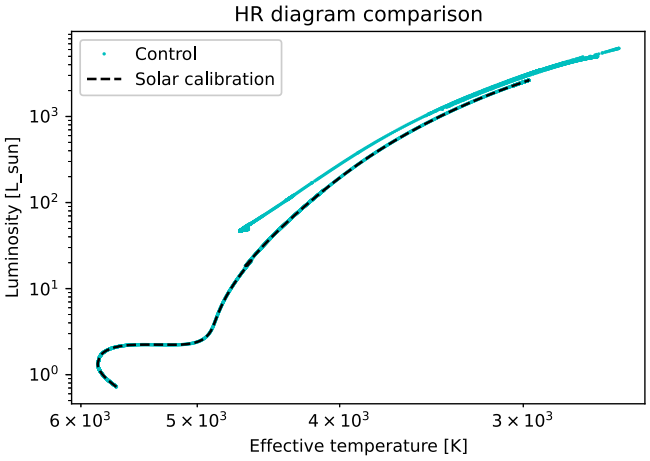

Figure 11. Comparison between the PARSEC stellar evolution tracks with $Z_{ini} = 0.017$ (Control) and $Z_{ini} = 0.01769$ (Solar calibration). The solar calibration track stops at the RGB tip.

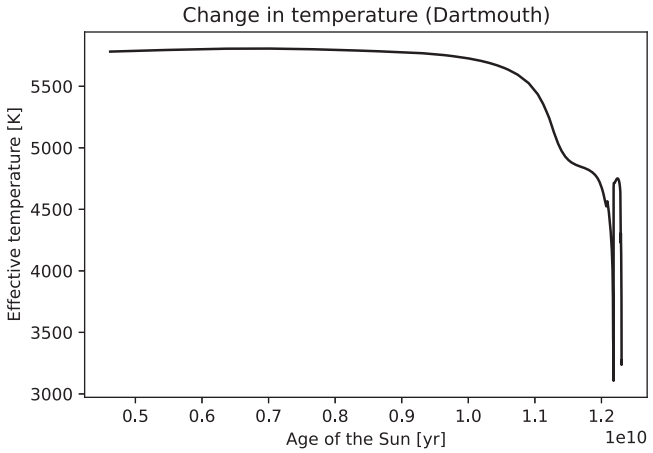

Figure 12. Effective temperature of the Sun (Dartmouth track) starting from the current age of the Sun until the end of the AGB phase.

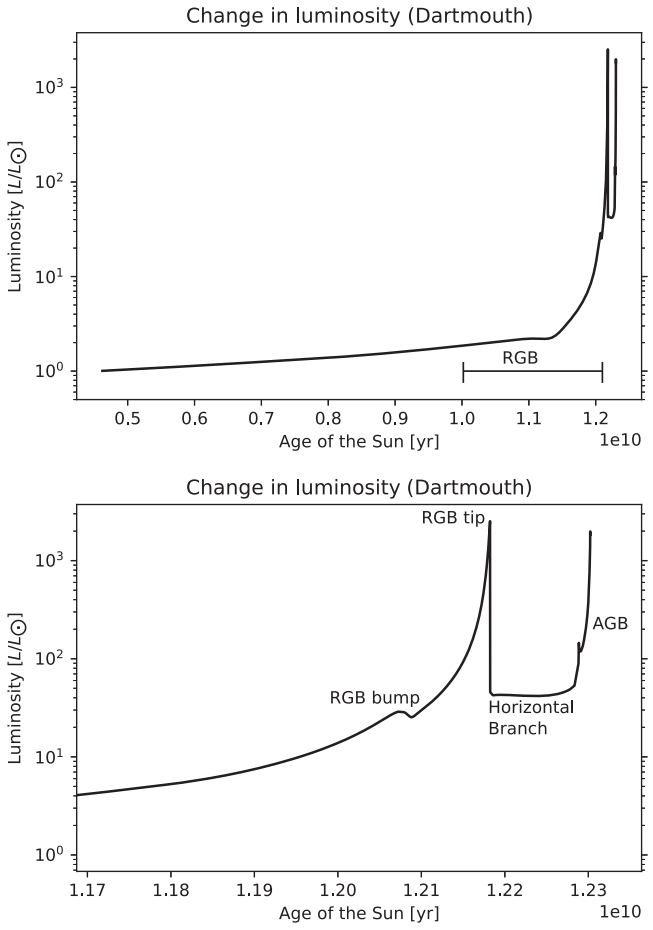

Figure 13. Evolution of luminosity for the Sun until the end of the AGB phase using the Dartmouth track. Upper panel: track starts from the current age of the Sun. The RGB is indicated with a span. Lower panel: zoom in near the end of the track. The "RGB bump" refers to the visual identification that the luminosity briefly decreases during the RGB phase. The "RGB tip" marks the end of the RGB phase.

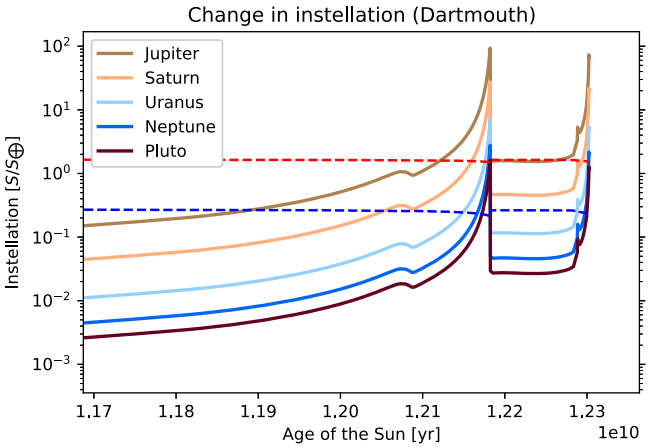

Figure 14. Instellation received at the top of the atmosphere of each of the outer planets as the Sun evolves during the RGB to the end of the AGB using the Dartmouth solar track. Dotted red and blue lines correspond to the instellation limit for the optimistic IHZ and OHZ, respectively.

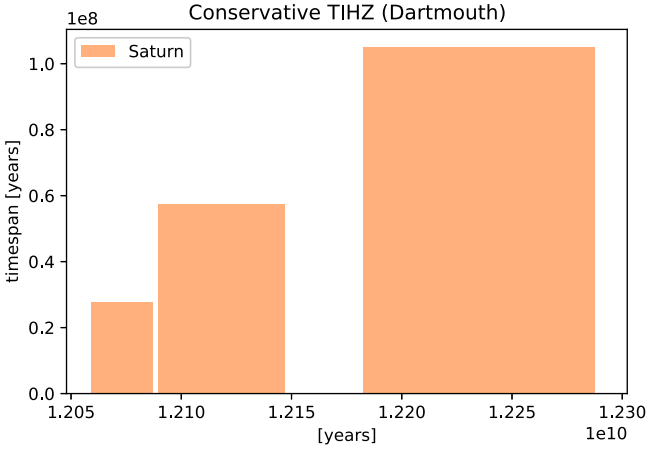

Figure 15. Size of the various TIHZs as well as times of occurrence for Saturn using the Dartmouth solar track and the conservative HZ definition. The first and second TIHZs are separated by 2 Myr of uninhabitability.

ORCID iDs

Viktor Sparrman https://orcid.org/0009-0007-7536-7455
Sara Bladh https://orcid.org/0000-0003-2964-7943
M. J. Way https://orcid.org/0000-0003-3728-0475

References

Bains, W. 2004, AsBio, 4, 137
Baraffe, I., Chabrier, G., Allard, F., & Hauschildt, P. H. 1998, A&A, 337, 403
Baraffe, I., Homeier, D., Allard, F., & Chabrier, G. 2015, A&A, 577, A42
Barnes, J. W., & O'Brien, D. P. 2002, ApJ, 575, 1087
Batygin, K., & Brown, M. E. 2016, AJ, 151, 22
Borucki, W. J., Koch, D., Basri, G., et al. 2010, Sci, 327, 977
Brown, M. E., & Batygin, K. 2016, ApJL, 824, L23
Carroll, B. W., & Ostlie, D. A. 2006, An Introduction to Modern Astrophysics and Cosmology (Reading, MA: Addison-Wesley Developers Press)
Catling, D. C., & Zahnle, K. J. 2020, SciA, 6, eaax1420
Charnay, B., Wolf, E. T., Marty, B., & Forget, F. 2020, SSRv, 216, 90
Coddington, O., Lean, J. L., Pilewskie, P., Snow, M., & Lindholm, D. 2016, BAMS, 97, 1265
Costa, G., Bressan, A., Mapelli, M., et al. 2021, MNRAS, 501, 4514
Costa, G., Girardi, L., Bressan, A., et al. 2019a, A&A, 631, A128
Costa, G., Girardi, L., Bressan, A., et al. 2019b, MNRAS, 485, 4641
Danchi, W. C., & Lopez, B. 2013, ApJ, 769, 27
Dearborn, D. S. P., Lattanzio, J. C., & Eggleton, P. P. 2006, ApJ, 639, 405
Dong, C., Huang, Z., Lingam, M., et al. 2017, ApJL, 847, L4
Dotter, A., Chaboyer, B., Jevremović, D., et al. 2007, AJ, 134, 376
Dotter, A., Chaboyer, B., Jevremović, D., et al. 2008, ApJS, 178, 89
Fortes, A. D. 2000, Icar, 146, 444
Fu, X., Bressan, A., Marigo, P., et al. 2018, MNRAS, 476, 496
Goldblatt, C., & Watson, A. J. 2012, RSPTA, 370, 4197
Goode, P. R., Qiu, J., Yurchyshyn, V., et al. 2001, GeoRL, 28, 1671
Grasset, O., Castillo-Rogez, J., Guillot, T., Fletcher, L. N., & Tosi, F. 2017, SSRv, 212, 835
Guo, J. H. 2019, ApJ, 872, 99
Haberle, R. M. 2022, Oxford Reference Encyclopedia of Planetary Science (Oxford: Oxford Univ. Press)
Harrington, R. S. 1988, AJ, 96, 1476
Hart, M. H. 1979, Icar, 37, 351
Heller, R., Williams, D., Kipping, D., et al. 2014, AsBio, 14, 798
Heller, R., & Zuluaga, J. I. 2013, ApJL, 776, L33
Howell, S. B., Sobeck, C., Haas, M., et al. 2014, PASP, 126, 398
Huang, S.-S. 1959, AmSci, 47, 397
Hunten, D. M., Pepin, R. O., & Walker, J. C. G. 1987, Icar, 69, 532
Iben, I. J. 1974, ARA&A, 12, 215
Ida, S., & Lin, D. N. C. 2004, ApJ, 604, 388
Ida, S., Ueta, S., Sasaki, T., & Ishizawa, Y. 2020, NatAs, 4, 880
Izidoro, A., Morbidelli, A., Raymond, S. N., Hersant, F., & Pierens, A. 2015, A&A, 582, A99
Jacobson, R. A., Antreasian, P. G., Bordi, J. J., et al. 2006, AJ, 132, 2520
Johnstone, C. P., Bartel, M., & Güdel, M. 2021, A&A, 649, A96
Kasting, J. F. 1991, Icar, 94, 1
Kasting, J. F., Whitmire, D. P., & Reynolds, R. T. 1993, Icar, 101, 108
Kleine, T., Budde, G., Burkhardt, C., et al. 2020, SSRv, 216, 1
Knoll, A. H., & Nowak, M. A. 2017, SciA, 3, e1603076
Koch, D. G., Borucki, W. J., Basri, G., et al. 2010, ApJL, 713, L79
Komatsu, E., Smith, K. M., Dunkley, J., et al. 2011, ApJS, 192, 18
Kopparapu, R. K., Ramirez, R., Kasting, J. F., et al. 2013, ApJ, 765, 131
Kopparapu, R. K., Ramirez, R. M., SchottelKotte, J., et al. 2014, ApJL, 787, L29
Kuramoto, K., Umemoto, T., & Ishiwatari, M. 2013, E&PSL, 375, 312
Lammer, H., Schiefer, S.-C., Juvan, I., et al. 2014, OLEB, 44, 239
Li, J., Jiang, J. H., Yang, H., et al. 2022, AJ, 163, 27
Lorenz, R. D., Lunine, J. I., & McKay, C. P. 1997, GeoRL, 24, 2905
Luger, R., Barnes, R., Lopez, E., et al. 2015, AsBio, 15, 57
Morbidelli, A., Tsiganis, K., Batygin, K., Crida, A., & Gomes, R. 2012, Icar, 219, 737
Nakajima, S., Hayashi, Y.-Y., Abe, Y., & Udalski, A. 1992, JAtS, 49, 2256
Nataf, D. M., Gould, A. P., Pinsonneault, M. H., & Udalski, A. 2013, ApJ, 766, 77
Nguyen, C. T., Costa, G., Girardi, L., et al. 2022, A&A, 665, A126
Pascal, R., Pross, A., & Sutherland, J. D. 2013, Open Biol. J., 3, 130156
Pizzolato, N., Maggio, A., Micela, G., Sciortino, S., & Ventura, P. 2003, A&A, 397, 147
Prialnik, D. 2000, An Introduction to the Theory of Stellar Structure and Evolution (Cambridge: Cambridge Univ. Press)
Pross, A., & Pascal, R. 2013, Open Biol. J., 3, 120190
Ramirez, R. M. 2018, Geosc, 8, 280
Ramirez, R. M., & Kaltenegger, L. 2016, ApJ, 823, 6
Ramirez, R. M., & Kaltenegger, L. 2018, ApJ, 858, 72
Ribas, I., Guinan, E. F., Güdel, M., & Audard, M. 2005, ApJ, 622, 680
Rybicki, K. R. 2006, PASP, 118, 1124
Saillenfest, M., Rogoszinski, Z., Lari, G., et al. 2022, A&A, 668, A108
Salaris, M., Cassisi, S., & Weiss, A. 2002, PASP, 114, 375
Salmon, J., & Canup, R. M. 2022, ApJ, 924, 6
Schopf, J. W., Kudryavtsev, A. B., Czaja, A. D., & Tripathi, A. B. 2007, PreR, 158, 141
Schulze-Makuch, D., & Irwin, L. N. 2001, EOSTr, 82, 150
Selsis, F., Kasting, J. F., Levrard, B., et al. 2007, A&A, 476, 1373
Sheppard, S. S., & Trujillo, C. 2016, AJ, 152, 221
Simpson, G. C. 1929, QJRMS, 55, 73
Solomon, S. C., & Head, J. W. 1991, Sci, 252, 252
Sparrman, V., Way, M., & Bladh, S. 2023, TIHZ calculator with water loss + Life probabilities + Stellar mass/metallicity comparison, , TIHZ calculator with water-loss + Life probabilities + Stellar mass/metallicity comparison, v1.2, Zenodo, doi:10.5281/zenodo.8272045
Spergel, D. N., Verde, L., Peiris, H. V., et al. 2003, ApJS, 148, 175
Stern, S. A. 2003, AsBio, 3, 317
Tanaka, K. L. 1986, JGR, 91, E139
Trujillo, C. A., & Sheppard, S. S. 2014, Natur, 507, 471
Tuchow, N. W., & Wright, J. T. 2021, RNAAS, 5, 194

Tuchow, N. W., & Wright, J. T. 2023, ApJ, 944, 71
Van Rossum, G., & Drake, F. L. 2009, Python 3 Reference Manual (Scotts Valley, CA: CreateSpace)
Walker, J. C. G., Hays, P. B., & Kasting, J. F. 1981, JGR, 86, 9776
Watson, A. J., Donahue, T. M., & Walker, J. C. G. 1981, Icar, 48, 150
Way, M. J., & Del Genio, A. D. 2020, JGRE, 125, e06276
Way, M. J., Del Genio, A. D., Aleinov, I., et al. 2018, ApJS, 239, 24
Way, M. J., Del Genio, A. D., Kiang, N. Y., et al. 2016, GeoRL, 43, 8376
Westall, F., Höning, D., Avice, G., et al. 2022, essoar, 10512790.1
Wilde, S. A., Valley, J. W., Peck, W. H., & Graham, C. M. 2001, Natur, 409, 175
Yang, J., Boué, G., Fabrycky, D. C., & Abbot, D. S. 2014, ApJL, 787, L2
Yang, J., Ding, F., Ramirez, R. M., et al. 2017, NatGe, 10, 556
Zhu, W., & Dong, S. 2021, ARA&A, 59, 291